JOURNAL OF AGRICULTURAL AND FOOD CHEMISTRY
ARTICLE

J. Agric. Food Chem. 2010, 58, 3753–3760 3753
DOI:10.1021/jf9033128

Composite Edible Films Based on Hydroxypropyl Methylcellulose Reinforced with Microcrystalline Cellulose Nanoparticles

Cristina Bilbao-Sáinz,* Roberto J. Avena-Bustillos Delilah F. Wood, Tina G. Williams, and Tara H. McHugh

Western Regional Research Center, Agricultural Research Service, U.S. Department of Agriculture, 800 Buchanan Street, Albany, California 94710

It has been stated that hydroxypropyl methyl cellulose (HPMC) based films have promising applications in the food industry because of their environmental appeal, low cost, flexibility and transparency. Nevertheless, their mechanical and moisture barrier properties should be improved. The aim of this work was to enhance these properties by reinforcing the films with microcrystalline cellulose (MCC) at the nano scale level. Three sizes of MCC nanoparticles were incorporated into HPMC edible films at different concentrations. Identical MCC nanoparticles were lipid coated (LC) prior to casting into HPMC/LC-MCC composite films. The films were examined for mechanical and moisture barrier properties verifying how the addition of cellulose nanoparticles affected the water affinities (water adsorption/desorption isotherms) and the diffusion coefficients. The expected reinforcing effect of the MCC was observed: HPMC/MCC and HPMC/LC-MCC films showed up to 53% and 48% increase, respectively, in tensile strength values in comparison with unfilled HPMC films. Furthermore, addition of unmodified MCC nanoparticles reduced the moisture permeability up to 40% and use of LC-MCC reduced this value up to 50%. Water vapor permeability was mainly influenced by the differences in water solubility of different composite films since, in spite of the increase in water diffusivity values with the incorporation of MCC to HPMC films, better moisture barrier properties were achieved for HPMC/MCC and HPMC/LC-MCC composite films than for HPMC films.

KEYWORDS: Hydroxypropyl methyl cellulose; microcrystalline cellulose; edible films; nanoparticles

INTRODUCTION

Edible films have long been used to prevent moisture, lipid, solute, or aroma compound migration between foods and their environments and also between different compartments in the same food (*1*). Previously, many research groups have developed new edible films. In general, it has been confirmed that proteins and polysaccharides, serving as structural matrices, have good mechanical properties and are excellent gas, aroma, and lipid barriers, but they have poor water vapor barrier properties. However, hydrophobic substances are good moisture barriers but form brittle films (*2*,*3*). Therefore, both substances have been combined to create composite barriers with desired mechanical strength and low permeability.

Cellulose-based edible films, such as hydroxypropyl methyl cellulose (HPMC), are widely reported in the literature (*4*−*8*). HPMC films tend to have moderate strength and are resistant to oils and fats, flexible, transparent, odorless, and tasteless (*9*). However, the water sensitivity of HPMC films, which produces a loss of barrier properties or even a solubilization into foods with high water activities, prevents their industrial applications. Some attempts have thus been made to incorporate hydrophobic substances into HPMC matrices to form composite films. A study of lipid type and amount of edible HPMC−lipid composite coating on oranges showed that beeswax exhibited the lowest weight loss (*10*). In different studies, the properties of HPMC-based films were improved by incorporating surfactants (*11*, *12*) and tea tree essential oil (*13*), but the challenge today is still the relatively high permeability and poor mechanical integrity of edible composite films.

One of the ongoing investigations to overcome this challenge concerns the use of cellulose fibers as reinforcing elements. The achievement of superior strength properties through the addition of cellulose fibers has been mentioned in several studies (*14*−*18*). However, the water absorbent nature of cellulose has been cited by many authors as providing a barrier to many potential applications involving cellulose-filled composite films. Previous work showed that cellulose fillers in sizes down to 500 nm increased the tensile strength 2-fold but did not improve the water vapor permeability of the HPMC films (*19*). The present work, in an effort to improve the water barrier properties, explores the effect of lipid-coated MCC fillers in the HPMC matrix. The objective of the work is, therefore, to complete the characterization of the composite HPMC/MCC films with and without modification of the MCC by lipid coating the nanoparticles. Food-grade

Published on Web 02/25/2010

MCC filler material was blended into films forming HPMC solutions at different ratios. The morphology and mechanical and water barrier properties of the ensuing composites were evaluated.

MATERIALS AND METHODS

Hydroxypropyl methyl cellulose (Methocel E15) was kindly provided by Dow Chemical Co. (Midland, MI.). HPMC was chosen as the film-forming agent because of its high film-forming properties and its compatibility with hydrophobic materials. Three different sizes of food grade unmodified MCC and lipid-coated (LC)-MCC nanoparticles were kindly provided by FMC Biopolymers (Princeton, NJ).

HPMC Film Solution. The outstanding property of HPMC gum is high viscosity at low concentrations; thus, only 3% w/w was necessary to provide the adequate viscosity of the film-forming solutions. The control film was prepared by dissolving HPMC in distilled water using a hot/cold technique. The powder was first dispersed by mixing thoroughly with one-fifth to one-third of the total volume of water and heated to above 90 °C until all nanoparticles were thoroughly hydrated. The balance of water was added as cold water to lower the dispersion temperature. Once the dispersion reaches 70 °C, HPMC becomes completely water solubilized.

HPMC/MCC Composite Film Solution. MCC samples were provided as 8% aqueous suspensions, and HPMC was mixed to the MCC suspension during the preparation of films to get final HPMC/MCC ratios in the dried films of 3:0.08, 3:0.4, and 3:0.8. The HPMC/water ratio in all films forming solutions was 3:97. These solutions were homogenized using a Polytron 3000 (Kinematica, Littau, Switzerland) at 10000 rpm for 20 min. The low surface energy of HPMC allows the incorporation of different quantities of hydrophobic nanoparticles, thus allowing film formation from all of the formulations. Vacuum was applied to degas the film solutions to prevent microbubble formation in the films. Glass casting plates (30 × 30 cm) with Mylar (polyester film, Dupont, Hopewell, VA) covers were used for film casting. The mixes were cast to a wet thickness of 1.15 mm onto plates using casting bars, and the plates were allowed to dry at room temperature for 24 h. After drying, the films were removed from the Mylar. Film thicknesses were measured to the nearest 0.001 mm at four positions around the film and in the center using a micrometer. Average values of five thickness measurements per film were used in all WVP calculations.

Particle Size Analysis. The size (as length) of the nanoparticles in solution was measured using a dynamic light scattering particle size analyzer (Malvern Zetasizer, Malvern Instruments Ltd., Westborough, MA). Scanning electron microscopy (SEM) was used to characterize the morphology of MCC nanoparticles in films and to measure the nanoparticles' diameter.

Water Vapor Permeability (WVP) Determination. The gravimetric modified cup method based on ASTM E96-80 was used to determine WVP. Cabinets used to test final films contain fans operated by motors and variable speed controllers. The cabinets were kept at 25.3 ± 0.8 °C. Fan speeds achieved air velocities of 500 ft/min (152 m/min) to ensure uniform relative humidity (RH) throughout the cabinets. Cabinets were pre-equilibrated to 0% RH using calcium sulfate desiccant. Test cups were made from poly(methyl methacrylate) (Plexiglas). A film was sealed to the cup base with a ring containing a 19.6 cm^2 opening using four screws symmetrically located around the cup circumference. Deionized water was placed in the bottom of the test cup to expose the film to a high water activity inside the test cups. The films in the cup were oriented with the shiny side (the film side originally in contact with the Mylar cover) facing down (toward the inner, high-RH environment of the cup). Average stagnant air gap heights between the water and the film were determined. At least eight test cups containing the same film were inserted into the pre-equilibrated 0% RH desiccator cabinets. Eight weights were taken for each cup at greater than 2 h intervals. For each experiment, the relative humidity at the film's underside and corrected WVP was calculated by the WVP correction method, accounting for the effect of the water vapor concentration gradient through the stagnant air layer in the cups (*20*).

Mechanical Property Measurements. After drying, the films were cut to have a rectangular midsection of 15 mm wide by 100 mm long, flaring to 25 mm by 35 mm square sections on each end. At least 16 replicates of each film were tested. The cut films were then conditioned at 33% RH for 72 h using a saturated solution of $MgCl_2$ at 23 ± 2 °C. This preconditioning before the tensile testing enables a true comparison of mechanical strength of the films.

An Instron Universal Testing Machine (model 1122, Instron Corp., Canton, MA) was used to determine the maximum TS (tensile strength) and maximum percentage elongation at break. The instrument was operated with self-alignment grips that consist of one fixed and one free end. The free end moves easily into alignment when load is applied. The mechanical properties were determined at 21 °C according to ASTM D882-97. The ends of the cut films were clamped with grips, and films were stretched using a speed of 50 mm/min.

The tensile strength is the maximum stress a film can withstand against applied tensile stress before the film tears. It is calculated by dividing the maximum load at break by the cross-sectional area of the film. Elongation at break is the percentage change in the original film length between the grips. The final length is measured when the film breaks.

Film Water Affinity. Water transfer through the film occurs in three steps: first, water vapor condenses and dissolves on the high water concentration side of the film surface; second, water molecules move through the film, driven by a concentration or activity gradient; and third, water evaporates from the other side of the film (*21*). Therefore, the factors describing the permeability process include the affinity between the water and the film material (adsorption/desorption) and the resistance of water movement in the polymeric network matrix, expressed as effective diffusivity (*22*−*24*).

A dynamic vapor sorption analyzer DVS-1 (Surface Measurement Systems, Allentown, PA) was used to obtain the water adsorption/desorption isotherms of selected formulations. Each film was subjected to various conditions of relative humidity, and the response of the sample was measured gravimetrically over time until the sample reached equilibrium. The sample was exposed to a humidity range of 0−98% and then 98−0% again at 25 °C. At least three replicates of each film were tested.

The Guggenheim−Anderson−de Boer (GAB) model (eq **1**) was used to represent the experimental equilibrium data. In this equation the parameter X_w is the equilibrium moisture (g of water/g of dry mass), m_0 is the monolayer water content, C is the Guggenheim constant, which represents the sorption heat of the first layer, and k is the sorption heat of the multilayer. The GAB model parameters were determined by polynomial regression using Microsoft Excel 2007.

$$X_w = \frac{C \times k \times m_0 \times a_w}{[(1 - ka_w) \times (1 - ka_w + Cka_w)]} \quad (1)$$

The method used to calculate the diffusion constants for the thin films uses diffusion equations first employed by Crank (*25*). At short times, the initial kinetics of sorption into the bulk may be described by eq **2**

$$\frac{M_t}{M_\infty} = \frac{4}{L}\sqrt{\frac{D \times t}{\pi}} \quad (2)$$

where M_t = mass of water sorbed at time t, M_∞ = mass sorbed at thermodynamic equilibrium, L is the thickness of the film, and D is the diffusion coefficient. A diffusion coefficient is calculated for every relative humidity step from the slope by fitting a line M_t/M_∞ versus sqrt (time)/d, keeping the fitted R^2 over 99%.

Scanning Electron Microscopy (SEM). Approximately 10 μL of each MCC solution was dropped onto a Mica disk (highest quality grade VI, Ted Pella, Inc., Redding, CA) previously attached to an aluminum specimen stub (Ted Pella, Inc.) with a double-adhesive coated carbon tab (Ultra Smooth Carbon Tabs, Electron Microscopy Sciences, Hatfield, PA). The solution was allowed to air-dry in a desiccator. Film surfaces were prepared for SEM by attaching the film directly to a stub with a carbon tab. Film cross sections were prepared by dropping a film into liquid nitrogen followed by fracturing with a prechilled razor held in a vise-grip locking pliers. The freshly fractured film pieces were retrieved from the liquid nitrogen bath and placed as quickly as possible into a Petri dish containing a piece of filter paper and placed in a desiccator to warm and dry to room temperature. Fractured film pieces were then mounted fractured surface up on a half-stub attached to a full stub using carbon tabs. Once the samples were secured to the SEM stubs, they were coated

with gold−palladium in a Denton Desk II sputter coating unit (Denton Vacuum U.S.A, Moorestown, NJ). All samples were then viewed and photographed in a Hitachi S-4700 field emission scanning electron microscope (Hitachi, Japan) at 2 kV.

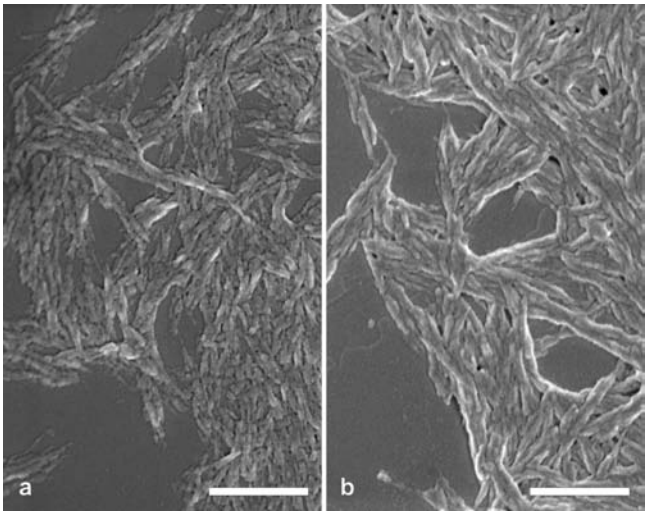

Figure 1. Scanning electron micrographs of microcrystalline cellulose (MCC) nanoparticles: (**a**) unmodified MCC; (**b**) lipid-coated MCC. Scale bars = 500 nm.

Table 1. MCC Nanoparticle Sizes

MCC sample	diameter (nm)	length (nm)
MCC1	31.8 ± 2.8	744 ± 73
MCC2	38.9 ± 2.4	870 ± 40
MCC3	42.2 ± 4.1	1000 ± 31
LC[a]-MCC1	40.5 ± 6.1	1210 ± 121
LC-MCC2	45.2 ± 5.3	1173 ± 40
LC-MCC3	48.1 ± 2.3	1186 ± 54

[a] Lipid coated.

Statistical Analysis of Data. Analysis of variance and multiple-comparison tests were applied using Minitab 14.2 (Minitab Inc., State College, PA) to study the significant effects of the HPMC/MCC ratio, nanoparticle size, and nanoparticle coating on film functional properties.

RESULTS AND DISCUSSION

Characterization of the Microcrystalline Cellulose Nanoparticles. The shape of filler nanoparticles is rod-like as shown in **Figure 1**, which shows SEM micrographs of the unmodified MCC (**Figure 1a**) and LC-MCC (**Figure 1b**). These micrographs show that the lipid-coated nanoparticles have a more continuous surface than their counterparts. Most of the cellulose nanoparticles appear to be aggregated, due to the highly polar surface of the cellulose fibers, which causes interfiber aggregations by hydrogen bonding forming bundles. The dimensions of the unmodified MCC and LC-MCC nanoparticles are reported in **Table 1**.

Mechanical Properties. Panels **a** and **b** of **Figure 2** show the results of tensile strength (TS) from all of the tests. The TS of the control sample was 35.6 ± 3.3 MPa. In agreement with our results, Sebti et al. (*26*) reported 32 ± 6 MPa for the tensile strength of films prepared from 3 wt % HPMC solution. Inclusion of unmodified MCC in the HPMC films resulted in an increase in TS values from about 36 to 53% as MCC content increased from 3:0.08 to 3:0.8 HPMC/MCC ratio. The TS values of the HPMC/MCC nanocomposite films were not influenced (no significant differences at $P > 0.05$) by nanoparticle size in the range studied. With respect to the hydrophobic nanoparticles, inclusion of LC-MCC did not always result in better tensile properties, but when the smallest LC-MCC1 was incorporated into the HPMC film at a low ratio (3:0.08), a 48% increase in TS with respect to the unfilled film was achieved. Increasing the nanoparticle size or the concentration decreased the TS values.

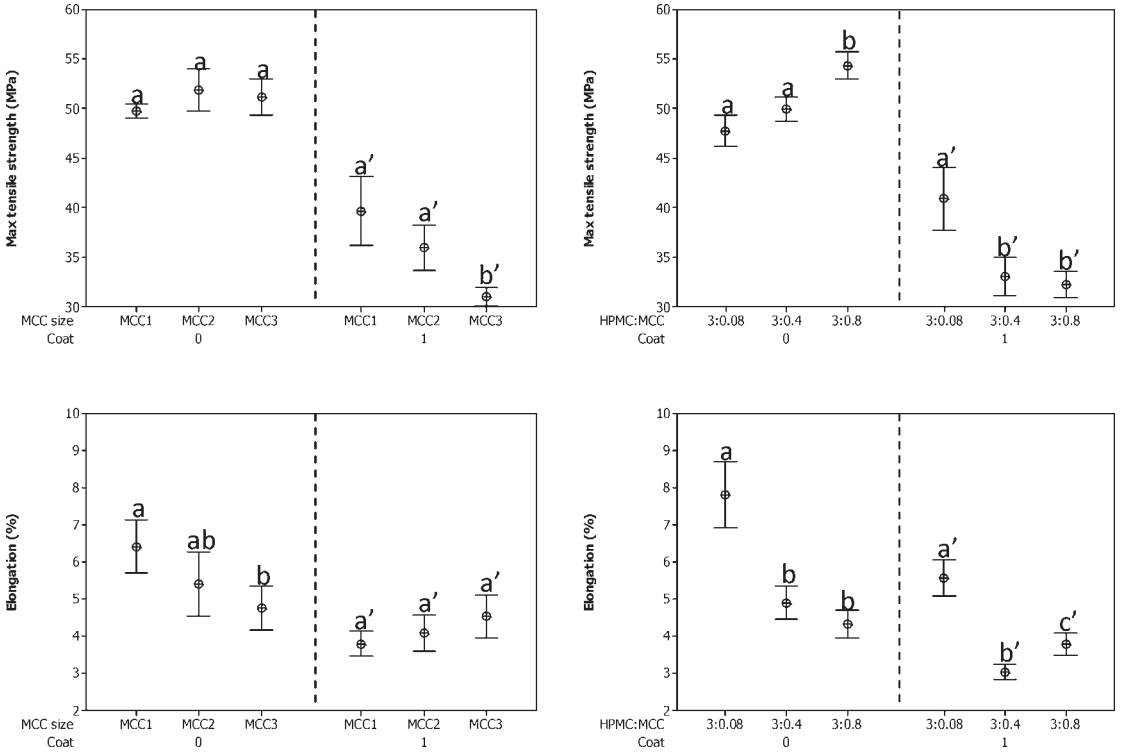

Figure 2. Maximum tensile strength of hydroxypropyl methylcellulose (HPMC) films compounded with different nanoparticle sizes (**a**) at different HPMC/MCC ratios (**b**). Elongation at break of HPMC films compounded with different nanoparticle size (**c**) at different HPMC/MCC ratios (**d**). 0, unmodified MCC; 1, lipid coated MCC. Data represent mean and 95% CI for the mean. Means with the same letters are not significantly different.

Table 2. Comparison of Water Vapor Permeability of HPMC Films Reinforced with Different Concentrations of MCC Nanoparticles

film type	HPMC/MCC ratio	thickness (mm)	RH (%) film underside	WVTR (g/h·m^2)	permeability (g·mm/kPa·h·m^2)
control (3 wt % HPMC)		0.026 ± 0.007	81 ± 2	46.0 ± 8.7	0.47 ± 0.04
HPMC/MCC1	3:0.08	0.020 ± 0.001	82 ± 1	44.1 ± 2.0	0.33 ± 0.02
	3:0.4	0.020 ± 0.002	83 ± 1	42.8 ± 2.5	0.32 ± 0.03
	3:0.8	0.020 ± 0.001	83 ± 1	41.9 ± 2.4	0.31 ± 0.02
HPMC/MCC2	3:0.08	0.020 ± 0.002	83 ± 1	42.7 ± 1.6	0.32 ± 0.02
	3:0.4	0.020 ± 0.004	83 ± 1	42.3 ± 2.2	0.30 ± 0.01
	3:0.8	0.025 ± 0.004	83 ± 2	41.6 ± 3.8	0.31 ± 0.01
HPMC/MCC3	3:0.08	0.019 ± 0.004	83 ± 2	42.8 ± 3.7	0.31 ± 0.02
	3:0.4	0.019 ± 0.002	83 ± 2	42.8 ± 3.9	0.30 ± 0.02
	3:0.8	0.019 ± 0.001	84 ± 1	40.0 ± 1.7	0.28 ± 0.02
HPMC/LC[a]-MCC1	3:0.08	0.020 ± 0.002	83 ± 1	42.9 ± 3.5	0.33 ± 0.03
	3:0.4	0.022 ± 0.002	87 ± 1	32.8 ± 1.6	0.26 ± 0.01
	3:0.8	0.020 ± 0.001	85 ± 1	37.3 ± 3.0	0.28 ± 0.01
HPMC/LC-MCC2	3:0.08	0.020 ± 0.002	83 ± 1	40.9 ± 2.3	0.31 ± 0.03
	3:0.4	0.021 ± 0.001	85 ± 1	36.5 ± 2.3	0.28 ± 0.02
	3:0.8	0.021 ± 0.001	86 ± 1	33.2 ± 1.3	0.25 ± 0.01
HPMC/LC-MCC3	3:0.08	0.021 ± 0.005	83 ± 2	41.0 ± 3.3	0.31 ± 0.02
	3:0.4	0.020 ± 0.002	84 ± 1	39.7 ± 3.2	0.31 ± 0.01
	3:0.8	0.021 ± 0.001	87 ± 1	30.9 ± 1.1	0.23 ± 0.01

[a] Lipid coated.

The tensile strength is largely dependent on the distribution and intensity of inter- and intramolecular interactions. Unmodified MCC nanoparticles have polar characteristics, interacting with the hydrophilic groups along the cellulose backbone of the HPMC molecules. These interactions can result in stronger interfacial adhesion between the unmodified MCC and the HPMC matrix, which leads to a higher efficiency of the stress transfer from the matrix to the fibers. In hydrophobic nanoparticle incorporation cases, the lipid coating of the cellulose fibers reduced the polar character of the MCC; weak hydrophobic interactions are expected between the lipid-coated nanoparticles and the methyl groups of the HPMC, reducing the interfacial adhesion between the inclusions and the matrix and therefore reducing the tensile strength of the composite films.

Panels **c** and **d** of **Figure 2** show the evolution of the elongation at break versus nanoparticle size and nanoparticle quantity. The elongation of the HPMC film without filler was 4.9 ± 1.3%. Preparation of film solutions with the addition of unmodified nanoparticles increased the elongation at break up to 90%. Smaller nanoparticles resulted in an increased elongation at break compared to that of larger nanoparticles. Dogan et al. (*19*) observed the same effect; addition of 1000 nm MCC particle size resulted in lower values of elongation at break in comparison with the control sample; however, addition of 500 nm particle size maintained the elongation at break at the level of the control samples. The authors attributed this effect to the increased interaction area of well-aligned and homogeneously dispersed MCC nanofibers exerting a plasticizing effect. The films extensibility was not improved when hydrophobic nanoparticles were incorporated; only low concentrations of LC-MCC caused a 15% increase in the elongation at break values with respect to the unfilled film. The decrease in the elongation at break values of HPMC/LC-MCC composite films in comparison to HPMC/MCC composite films can be due to a lower continuity of the HPMC network due to the lipid coating of the MCC nanoparticles because incorporation of lipids provokes structural discontinuities and reduces the resistance to fracture of the film.

Effect of Fillers on Water Vapor Permeability of Composite Films. The effect of nanoparticle type, size, and concentration on water vapor permeability (WVP) of HPMC films was studied. Water vapor transmission rate (WVTR) and WVP values of films with various MCC sizes and contents are given in **Table 2**, where film thickness and relative humidity at the underside of the film are also included. WVP is probably the most informative parameter because it takes both the water vapor pressure difference between the two sides of the film and the film thickness into account. To show graphically the significance of the nanoparticle size and content, the interval plot of WVP versus MCC size and content at 95% confidence interval (CI) for the mean are shown in **Figure 3**.

The WVP of the control HPMC film with no particle inclusions was 0.47 ± 0.04 g·mm/kPa·h·m^2. The data presented in **Table 2** and **Figure 3** show that for unmodified MCC, a tendency to a lower permeability was observed with increasing MCC concentration. This behavior was attributed to the low hygroscopicity of the crystalline cellulose nanoparticles because moisture transfer preferentially occurs through noncrystalline areas. A significant improvement in WVP was obtained by adding commercial cellulose fibers or microfibers to starch films by other authors (*17*, *27*). They related the lower WVP to the highly crystalline "hydrophobic" character of the cellulose fibers in comparison to the hydrophilic starch films. An improvement in water resistance was also noted for LC-MCC; however, the percent reduction in WVP with added nanoparticles was greater for LC-MCC than for the unmodified MCC due to the apolar nature of LC-MCC, which decreases the moisture affinity of films.

In accordance with our results, it is reported in the literature that a decrease in WVP with an increased concentration of lipid in cellulose-based films was obtained (*6*, *28*, *29*). However, in contrast to what is found by other authors, no evident improvement in film resistance to water vapor transfer when decreasing nanoparticle size has been noted as it is often presented in correlation with an increase in the tortuosity within the film (*19*, *30*, *31*). On the contrary, WVP decreased as nanoparticle size increased in the range studied.

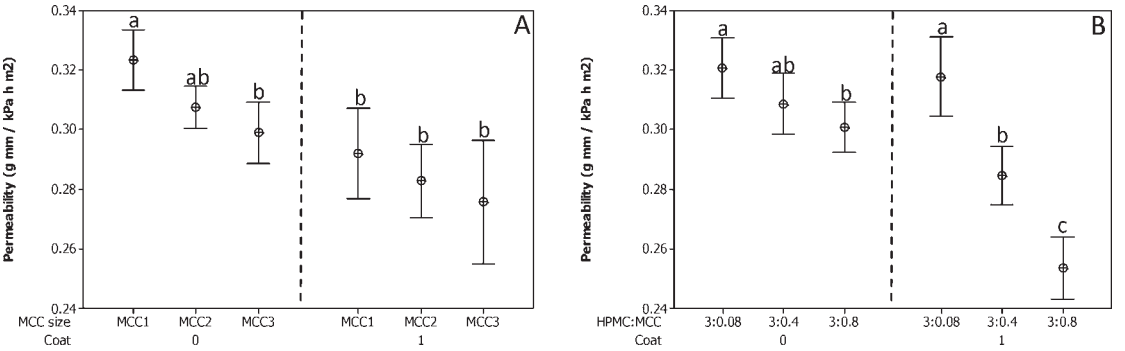

Figure 3. Effect of (**A**) nanoparticle size and (**B**) nanoparticle concentration on water vapor permeability of HPMC-based films. 0, unmodified MCC; 1, lipid-coated MCC. Data represent mean and 95% CI for the mean. Means with the same letters are not significantly different.

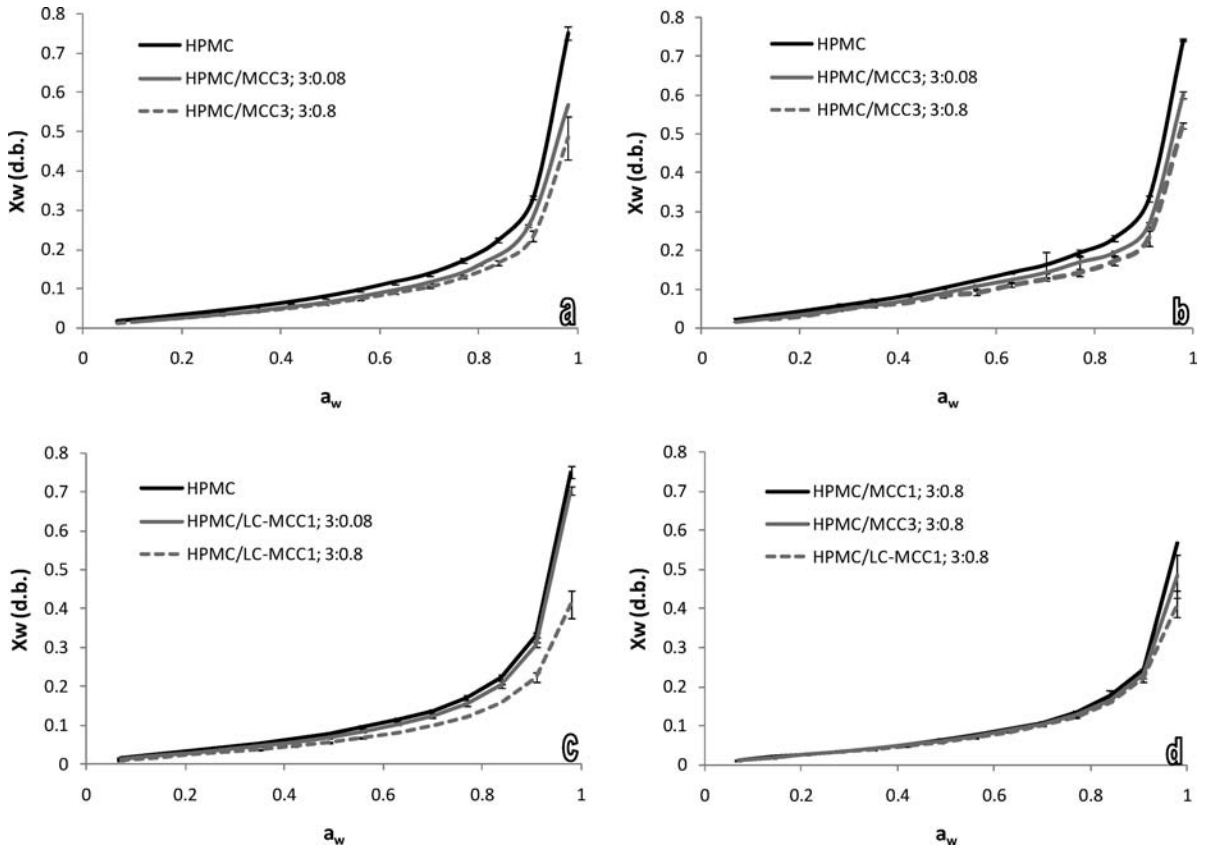

Figure 4. Experimental data showing (**a**) effect of microcrystalline cellulose (MCC) content on water adsorption isotherms, (**b**) effect of MCC content on water desorption isotherms, (**c**) effect of lipid-coated MCC (LC-MCC) content on water adsorption isotherms, and (**d**) effect of MCC size and coating on water adsorption isotherms.

Water Adsorption/Desorption Isotherms of HPMC-Based Films. The mass transfer process was investigated by obtaining the water adsorption/desorption isotherm (equilibrium moisture content on a dry basis versus water activity) of the composite films at 25 °C. The adsorption/desorption isotherms are displayed in **Figure 4**, which also includes the isotherm obtained for the unfilled HPMC films as a reference.

The water adsorption/desorption curves of HPMC-based films are sigmoid in shape, showing a slower increase in equilibrium moisture content until $a_w = 0.7$, after which a small increase in humidity led to a large mass gain, suggesting a swelling phenomenon as water activity increased and promoted solubilization. Similar behavior was observed by other authors for HPMC-based films (*5*, *12*, *13*, *28*).

Panels **a** and **b** of **Figure 4** show that HPMC films have the highest water affinity due to the large amount of hydrophilic groups. HPMC/MCC and HPMC/LC-MCC composite films showed flatter adsorption/desorption isotherms compared to pure HPMC films in the complete range of a_w, showing lower water-binding capacity with increased MCC nanoparticles. The lower water-binding capacity could be due to interactions between the MCC and the hydrophilic sites of the HPMC chain, which substitute the HPMC−water interactions that predominate in films without inclusions. The results shown in **Figure 4** agree with the work of others on composites of starch and cellulose fibers (*32*−*35*). Water uptake in the high a_w range was slightly higher for smaller particle sizes than for greater particle sizes as it was also slightly higher for HPMC/MCC composite films than for HPMC/LC-MCC films (**Figure 4d**). The lipid coating of the MCC could account for the reduction in water uptake because it may have protected the surface by decreasing moisture uptake by the nanoparticles.

Table 3. GAB Model Fitted Parameters for Sorption Data from HPMC Films with Incorporation of MCC Nanoparticles at Different HPMC/MCC Ratios

	GAB parameters			
sample	m_0 (g of water/g of solid)	C	K	R^2
HPMC	0.052 ± 0.003	4.86 ± 0.26	0.942 ± 0.011	0.969 ± 0.018
3 HPMC/0.08 MCC1	0.044 ± 0.003	3.87 ± 0.34	0.937 ± 0.021	0.988 ± 0.002
3 HPMC/0.8 MCC1	0.043 ± 0.005	4.78 ± 0.51	0.949 ± 0.015	0.980 ± 0.003
3 HPMC/0.08 MCC3	0.046 ± 0.001	3.82 ± 0.06	0.927 ± 0.002	0.980 ± 0.007
3 HPMC/0.8 MCC3	0.041 ± 0.001	4.90 ± 0.19	0.927 ± 0.005	0.979 ± 0.001
3 HPMC/0.08 LC[a]-MCC1	0.046 ± 0.001	4.65 ± 0.12	0.949 ± 0.002	0.986 ± 0.004
3 HPMC/0.8 LC-MCC1	0.039 ± 0.002	4.82 ± 0.03	0.930 ± 0.017	0.985 ± 0.004

[a] Lipid coated.

The GAB model was used to fit the water adsorption data of the films in the entire a_w range. **Table 3** summarizes the constants for the GAB equation. The GAB model fit the film adsorption data very well as previously reported (*12*, *22*, *23*, *26*). The value of the monolayer water content (m_0) is of particular interest as it indicates the amount of water that is strongly adsorbed to specific sites and is considered to be the optimum value at which the film is most stable. The effect of MCC nanoparticle inclusion on film hygroscopicity could also be observed from the monolayer water content data, which was 0.052 g/g (db) for HPMC films without filler and decreased significantly ($p \leq 0.05$) with increasing filler content down to 0.039 g/g (db). The monolayer moisture content tended to decrease when hydrophobic MCC nanoparticles were incorporated into HPMC films, although this decrease was not statistically significant.

The constant C, related to the total heat sorption, decreased significantly with the incorporation of a low concentration of unmodified nanoparticles. The decrease in C seemed to indicate that water molecules are adsorbed with less energy into the active sites in composite HPMC/MCC films than in unfilled films.

Effective Water Diffusion Coefficient in Films. The values obtained for diffusion coefficients were between 10^{-9} and 10^{-8} cm^2/s (**Figure 5**), which are similar to values reported for many food products including gelatin, starch, and cellophane with water contents of 8−15 g/100 g (db) (*36*).

A decrease in water diffusivity with increasing moisture content was observed. According to Debeaufort et al. (*37*), these results may be explained by a clustering phenomenon. Once a monolayer of water molecules moistens the film, a further increase in moisture results in "free water" that does not interact with the polymer. The free water molecules aggregate to form di-, tri-, and tetramer clusters. The molecular volume of these clusters is larger than that of monomers and results in decreased diffusion.

Incorporation of MCC particles into HPMC films resulted in an increase in the diffusion coefficient of HPMC/MCC films. The larger diffusion coefficient could be due to the increased porosity of the HPMC matrix with MCC incorporation, which, in turn, could lead to capillary flow involving vapor diffusion through pores in the HPMC/MCC matrix.

Results do not show significant differences between diffusivities of films with different nanoparticle sizes. Thus, the water transfer mechanism in this system is independent of MCC nanoparticle size of those tested. However, HPMC/LC-MCC films showed slightly higher diffusivity values than HPMC/MCC films. The more hydrophobic LC-MCC nanoparticles in the HPMC film act as a driving force for the diffusion due to the high incompatibility of lipid with water molecules. Lipids can also have plasticizer properties that improve flexibility through increased mobility of the adjacent hydrocolloid chains. Chao and Rizvi (*38*) showed that plasticizers increase the number and size of cavities in the polymers, making diffusion easier.

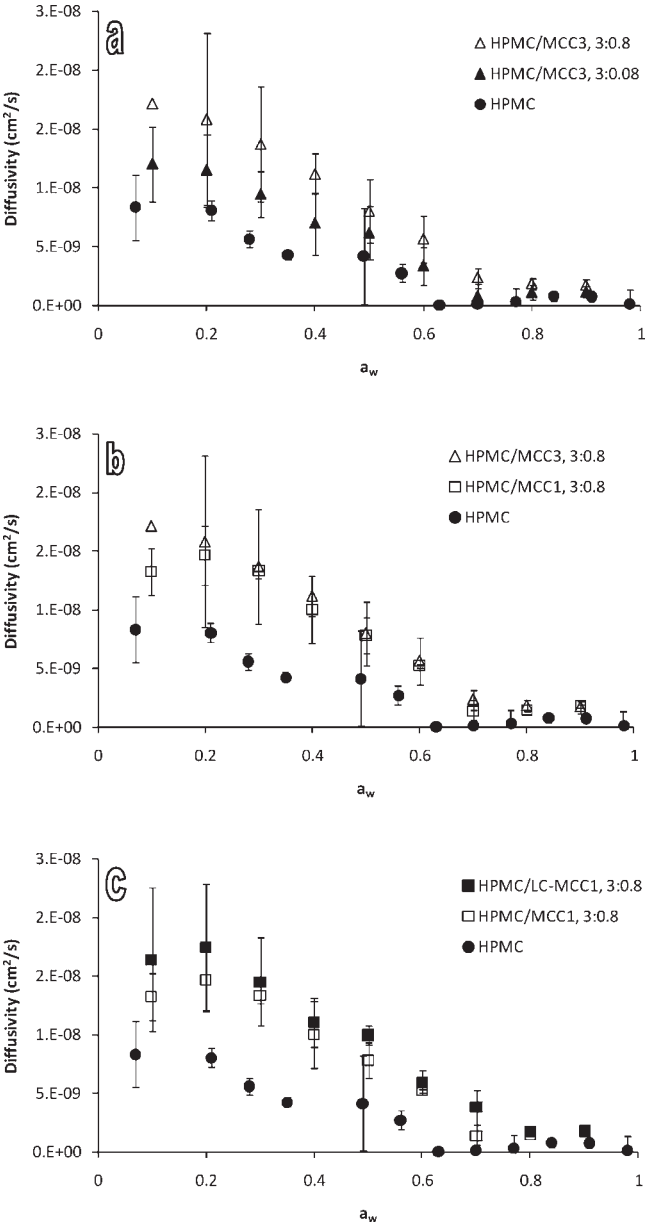

Figure 5. Effect on the water diffusion coefficient of hydroxypropyl methylcellulose (HPMC)-based films of (**a**) microcrystalline cellulose (MCC) content, (**b**) MCC nanoparticle size, and (**c**) lipid coating of the MCC nanoparticles.

Scanning Electron Microscopy of HPMC-Based Films. The permeability of films can be affected by the structure, morphology, and homogeneity (*39*) of the matrix. SEM was used to characterize the morphology of the composite films. **Figure 6**

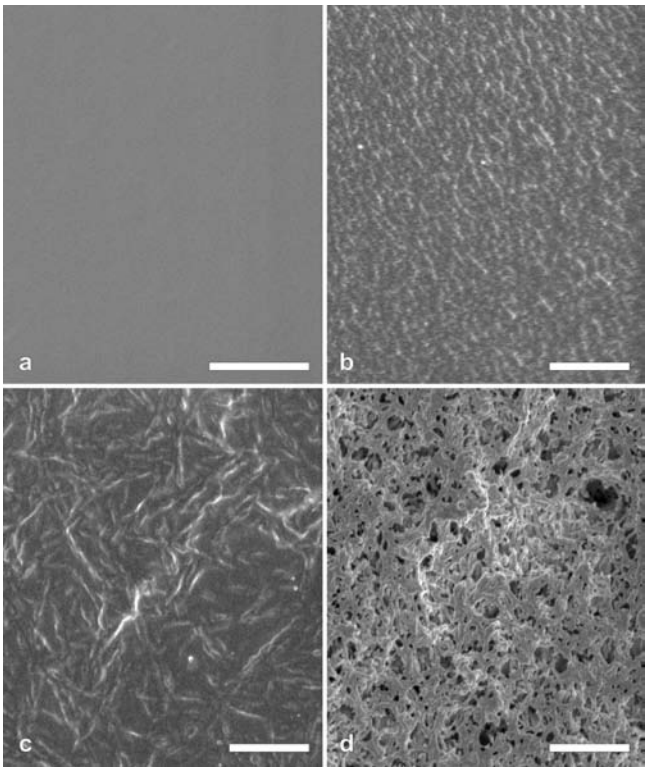

Figure 6. Scanning electron micrographs of (**a**) HPMC film surface, (**b**) HPMC cross section, (**c**) HPMC/MCC1 (3:0.8) film surface, and (**d**) HPMC/MCC1 (3:0.8) film cross section. HPMC, hydroxypropyl methylcellulose; MCC, microcrystalline cellulose. Scale bars: **a**, 500 nm; **b**−**d**, 1 μm.

shows surface features and cross sections of the unfilled and MCC-reinforced HPMC films.

The MCC nanoparticles appear lighter than the surrounding matrix and, thus, are readily identifiable in the films. The HPMC matrix displays a relatively smooth surface (**Figure 6a**), whereas the matrix in the nanocomposite films is rougher (**Figure 6c**). The filler is evenly distributed within the polymeric matrix; however, some of the nanoparticles are aggregated.

In the cross section, the unfilled and filled HPMC films show remarkable differences. Whereas a continuous structure was observed for the unfilled HPMC films (**Figure 6b**), the nanocomposite HPMC/MCC film is not uniform, with fibrillar zones and holes (**Figure 6d**). The fracture surface of the nanocomposite HPMC/LC-MCC films displayed a similar nonuniform aspect (not shown). The presence of holes at the fractured surface could be due to entrapped air in the film during the evaporation step despite degassing of the suspension.

The structural data correlate well with the diffusivity values and confirm the presence of a more open network in the HPMC/MCC composite films, which could lead to changes in the water transfer mechanisms controlling the barrier properties of the reinforced films.

Conclusions. HPMC can be used in edible films and coatings because of its excellent film-forming properties and its compatibility with hydrophobic materials to form emulsions. In this study, composite materials were obtained by compounding unmodified and LC-MCC nanoparticles with HPMC.

Incorporation of unmodified MCC appreciably reinforced the HPMC matrix, regardless of the nanoparticle size. However, the reinforcing effect of the hydrophobic nanoparticles was limited, especially because of the lipid coating that hinders the stress transfer at the filler/matrix interface. HPMC/LC-MCC composite films exhibited lower values of tensile strength than unfilled HPMC films with the exception of the films reinforced with low concentrations of the smallest LC-MCC nanoparticles, which showed an increase of up to 48% in TS values.

Incorporation of MCC nanoparticles in HPMC film systems exhibited water barrier properties that improved with increasing size and quantity of MCC. The lipid coating of the MCC resulted in further improvement of the water barrier properties compared to unmodified MCC. The water affinity was the factor with the greatest influence on the water barrier properties. The addition of MCC in the HPMC matrix resulted in a decrease of its hydrophilic character and capacity to take up water, especially for hydrophobic nanoparticles. Therefore, compared to unfilled HPMC films, the low hydrophilicity of the MCC and LC-MCC counteracted the increase in water diffusivity through the more open-structured matrix, which led to an overall improvement of the moisture barrier properties of the composite films.

ACKNOWLEDGMENT

We thank Dr. Mike Cammarata and his research group at FMC Biopolymers R&D for providing the MCC samples.

LITERATURE CITED

(1) Kamper, S. L.; Fennema, O. R. Use of edible films to maintain water vapor gradients in foods. *J. Food Sci.* **1985**, *50*, 382–384.

(2) Hernández, E. Edible coatings from lipids and resins. In *Edible Coatings and Films to Improve Food Quality*; Krochta, J. M., Baldwin, E. A., Nisperos-Carriedo, M., Eds.; Technomic Publishing: Lancaster, PA, 1994; pp 279−303.

(3) Kester, J. J.; Fennema, O. R. Edible films and coatings: a review. *Food Technol.* **1986**, *40* (12), 47–49.

(4) Sothornvit, R. Effect of Hydroxypropyl methylcellulose and lipid on mechanical properties and water vapor permeability of coated paper. *Food Res. Int.* **2009**, *42* (2), 307–311.

(5) Sebti, I.; Chollet, E.; Degraeve, P.; Noel, C.; Peyrol, E. Water sensitivity, antimicrobial, and physicochemical analyses of edible films based on HPMC and/or chitosan. *J. Agric. Food Chem.* **2007**, *55*, 693–699.

(6) Ayranci, E.; Tunc, S. The effect of fatty acid content on water vapor and carbon dioxide transmissions of cellulose-based edible films. *Food Chem.* **2001**, *72*, 231–236.

(7) Quezada-Gallo, J. A.; Debeaufort, F.; Callegarin, F.; Voilley, A. Lipid hydrophobicity, physical state and distribution effects on the properties of emulsion-based edible films. *J. Membr. Sci.* **2000**, *180*, 37–46.

(8) Kamper, S. L.; Fennema, O. R. Water vapor permeability of edible bilayer films. *J. Food Sci.* **1984**, *49*, 1478−1481, 1485.

(9) Krochta, J. M.; Mulder-Johnston, C. Edible and biodegradable polymer films: challenges and opportunities. *Food Technol.* **1997**, *51*, 61–74.

(10) Pérez-Gago, M. B.; Rojas, C.; del Rio, M. A. Effect of lipid type and amount of edible hydroxypropyl methylcellulose-lipid composite coatings used to protect postharvest quality of mandarins cv. Fortune. *J. Food Sci.* **2002**, *67* (8), 2903–2910.

(11) Villalobos, R.; Chanona, J.; Hernández, P.; Gutiérrez, G.; Chiralt, A. Gloss and transparency of hydroxypropyl methyl cellulose films containing surfactants as affected by their microstructure. *Food Hydrocolloids* **2005**, *19*, 53–61.

(12) Villalobos, R.; Hernández-Muñoz, P.; Chiralt, A. Effect of surfactants on water sorption and barrier properties of hydroxypropylmethylcellulose films. *Food Hydrocolloids* **2006**, *20*, 502–509.

(13) Sánchez-González, L.; Vargas, M.; González-Martínez, C.; Chiralt, A.; Cháfer, M. Characterization of edible films based on hydroxypropylmethylcellulose and tea tree essential oil. *Food Hydrocolloids* **2009**, 1–8.

(14) Teixeira, E. de M.; Pasquini, D.; Curvelo, A. A. S.; Corradini, E.; Belgacem, M. N.; Dufresne, A. Cassava bagasse cellulose nanofibrils reinforced thermoplastic cassava starch. *Carbohydr. Polym.* **2009**, doi: 10 1016/I carbpol 2009 04 034.

(15) Freire, C. S. R.; Silvestre, A. J. D.; Pascoal-Neto, C.; Gandini, A.; Martin, L.; Mondragon, I. Composite based on acylated cellulose fibers and low-density polyethylene: effect of the fiber content, degree of substitution and fatty acid chain length on final properties. *Compos. Sci. Technol.* **2008**, *68*, 3358–3364.
(16) Angles, M. N.; Dufresne, A. Plasticized starch/tunicin whisker nanocomposites. 1. Structural analysis. *Macromolecules* **2000**, *33*, 8344–8353.
(17) Dufresne, A.; Dupeyre, D.; Vignon, M. R. Cellulose microfibrils from potato tuber cells: processing and characterization of starch-cellulose microfibril composites. *J. Appl. Polym. Sci.* **2000**, *76*, 2080–2092.
(18) Favier, V.; Cavaille, J. Y.; Canova, G. R.; Shrivastava, S. C. Mechanical percolation in cellulose whisker nanocomposites. *Polym. Eng. Sci.* **1995**, *37* (10), 1732–1739.
(19) Dogan, N.; McHugh, T. H. Effects of microcrystalline cellulose on functional properties of hydroxypropyl methyl cellulose microcomposite films. *J. Food Sci.* **2007**, *72* (1), E16–E22.
(20) McHugh, T. H.; Avena-Bustillos, R.; Krochta, J. M. Hydrophilic edible films: Modified procedure for water vapor permeability and explanation of thickness effects. *J. Food Sci.* **1993**, *58*, 899–903.
(21) Krochta, J. M.; Miller, K. S. Oxygen and aroma barrier properties of edible films: a review. *Trends Food Sci. Technol.* **1997**, *8*, 228–237.
(22) Müller, C. M. O.; Laurindo, J. B.; Yamashita, F. Effect of cellulose fibers addition on the mechanical properties and water vapor barrier of starch-based films. *Food Hydrocolloids* **2009**, *23*, 1328–1333.
(23) Müller, C. M. O.; Yamashita, F.; Laurindo, J. B. Evaluations of the effect of glycerol and sorbitol concentration and water activity on the water barrier properties of cassava starch films through a solubility approach. *Carbohydr. Polym.* **2008**, *72*, 82–87.
(24) Larotonda, F. D. S.; Matsui, K. N.; Sobral, P. J. A.; Laurindo, J. B. Hygroscopicity and water vapor permeability of Kraft paper impregnated with starch acetate. *J. Food Eng.* **2005**, *71*, 394–402.
(25) Crank, J. *The Mathematics of Diffusion*, 2nd ed.; Clarendon Press: Oxford, U.K., 1975.
(26) Sebti, I.; Delves-Broughton, J.; Coma, V. Physicochemical properties and bioactivity of nisin-containing cross-linked hydroxypropylmethylcellulose films. *J. Agric. Food Chem.* **2003**, *51*, 6468–6474.
(27) Funke, U.; Bergthaller, W.; Lindhauer, M. G. Processing and characterization of biodegradable products based on starch. *Polym. Degrad. Stability* **1998**, *59*, 293–296.
(28) Sebti, I.; Ham-Pichavant, F.; Coma, V. Edible bioactive fatty acid-cellulosic derivative composites used in food-packaging applications. *J. Agric. Food Chem.* **2002**, *50*, 4290–4294.
(29) Hagenmaier, R. D.; Shaw, P. E. Moisture permeability of edible films made with fatty acid and hydroxypropylmethylcellulose. *J. Agric. Food Chem.* **1990**, *38*, 1799–1803.
(30) Pérez-Gago, M. B.; Krochta, J. M. Lipid particle size effect on water vapor permeability and mechanical properties of whey protein/beeswax emulsion films. *J. Agric. Food Chem.* **2001**, *49*, 996–1002.
(31) Debeaufort, F.; Voilley, A. Effect of surfactants and drying rate on barrier properties of emulsified edible films. *Int. J. Food Sci. Technol.* **1995**, *30*, 183–190.
(32) Ma, X.; Yu, J.; Kennedy, J. F. Studies on the properties of natural fibers-reinforced thermoplastics starch composites. *Carbohydr. Polym.* **2005**, *62*, 19–24.
(33) Avérous, L.; Fringant, C.; Moro, L. Plasticized starch−cellulose interactions in polysaccharides composites. *Polymer* **2001**, *42*, 6565–6572.
(34) Curvelo, A. A. S.; de Carvalho, A. J. F.; Agnelli, J. A. M. Thermoplastic starch−cellulosic fibers composites: preliminary results. *Carbohydr. Polym.* **2001**, 45, 183−188.
(35) Dufresne, A.; Vignon, M. R. Improvement of starch films performance using cellulose microfibrils. *Macromolecules* **1998**, *31*, 2693–2696.
(36) Bruin, S.; Luyben, K. C. A. M. Drying in food materials: a review of recent developments. In *Advances in Drying*; Mujumbar, A., Ed.; Hemisphere Publishing: Bristol, PA, 1980; Vol. 1.
(37) Debeaufort, F.; Voilley, A.; Meares, P. Water vapor permeability and diffusivity through methylcellulose edible films. *J. Membr. Sci.* **1994**, *91*, 125–133.
(38) Chao, R. R.; Rizvi, H. H. Oxygen and water vapor transport through polymeric film. A review of modeling approaches. In *Food and Packaging Interactions*; Hotchkiss, J. H., Ed.; American Chemical Society: Washington, DC, 1988; pp 216−242.
(39) McHugh, T. H.; Krochta, J. M. Permeability properties of edible films. In *Edible Coatings and Films to Improve Food Quality*; Krochta, J. M., Baldwin, E. A., Nisperos-Carriedo, M., Eds.; Technomic Publishing: Lancaster, PA, 1994; pp 139−187.

Received for review September 18, 2009. Revised manuscript received December 16, 2009. Accepted January 5, 2010. Thanks are due to XL TechGroup for financial support of this research.